Available online at www.sciencedirect.com
SCIENCE DIRECT
Journal of Catalysis 237 (2006) 237–247
JOURNAL OF CATALYSIS
www.elsevier.com/locate/jcat

The positive effect of NO on the N_2O decomposition activity of Fe-ZSM-5: A combined kinetic and in situ IR spectroscopic study

Gerhard D. Pirngruber [a,*], Johannis A.Z. Pieterse [b]

[a] *Institute for Chemical and Bioengineering, Swiss Federal Institute of Technology (ETH), Zürich, Wolfgang-Pauli Str. 10, CH-8093 Zürich, Switzerland*
[b] *ECN Clean Fossil Fuels, P.O. Box 1, Westerduinweg 3, NL-1755 ZG Petten, The Netherlands*

Received 19 September 2005; revised 11 November 2005; accepted 13 November 2005

Abstract

NO-assisted N_2O decomposition over four different Fe-ZSM-5 samples prepared by wet ion exchange (WIE) or chemical vapor deposition (CVD) of $FeCl_3$ was investigated by steady-state kinetics, in situ infrared (IR) spectroscopy, and transient response methods. Despite their lower iron loading, the samples prepared by WIE had the highest activity for N_2O decomposition in the presence of NO. The in situ IR experiments showed that the most active sample was characterized by a high concentration of adsorbed NO, as well as adsorbed NO_2 under reaction conditions. Step response experiments proved that NO_2 is an intermediate of the catalytic cycle and functions as intermediate oxygen storage. IR and transient kinetic experiments showed that WIE catalysts behave qualitatively different in NO-assisted N_2O decomposition than CVD catalysts. These differences are discussed in terms of the different structure of the iron species in the two types of samples.

Keywords: Fe-ZSM-5; CVD; Wet ion exchange; N_2O decomposition; NO; In situ IR; Step response; Pulse response

1. Introduction

N_2O emissions make a major contribution (6%) to the global greenhouse effect [1]. A considerable fraction of the total N_2O emissions are caused by the chemical industry in adipic acid and nitric acid plants. Abatement of these emissions by catalytic decomposition of N_2O is an important issue. Noble metal catalysts have very high intrinsic activities for N_2O decomposition [2]. But in the exhaust gas stream of adipic and nitric acid plants, N_2O is present together with NO and other components, such as O_2, H_2O, and so on. Most noble metal catalysts are strongly deactivated by the presence of these other components, particularly NO [3,4]. Iron zeolites show the opposite behavior, with N_2O decomposition activity strongly influenced by the presence of NO in the feed. This was originally attributed to a stoichiometric reaction of NO with N_2O, yielding N_2 and NO_2 [5], but later it was shown that NO has a truly catalytic effect on the N_2O decomposition activity [6]. Small amounts of NO increased N_2O conversion more than stoichiometrically. A redox mechanism with nitrites and nitrates as the redox species was given, but no spectroscopic evidence was provided:

$$N_2O + {}^*\text{–}NO_3^- \rightarrow {}^*\text{–}NO_2^- + N_2 + O_2, \quad (1)$$

$$N_2O + {}^*\text{–}NO_2^- \rightarrow N_2 + {}^*\text{–}NO_3^-. \quad (2)$$

Mul et al. [7] observed that a small amount of NO led to an increase in the conversion of N_2O by significantly more than one N_2O per NO added (as would be the case for the stoichiometric reaction). The effect of NO was explained by a different model [8]: NO that is adsorbed on the catalyst reacts with the oxygen atom that N_2O deposits on the catalyst surface and forms adsorbed NO_2. Thereby, the site for the activation N_2O is liberated, and a second oxygen atom from N_2O is deposited there. O_2 desorption occurs by recombination of the second deposited oxygen atom with an oxygen atom from NO_2. The following reaction equations show that the role of NO in the cycle in purely catalytic; it functions as an intermediate storage for deposited oxygen atoms:

$$^* + N_2O \rightarrow {}^*\text{–}O + N_2, \quad (3)$$

$$^*\text{–}O + {}^*\text{–}NO \rightarrow {}^* + {}^*\text{–}NO_2, \quad (4)$$

* Corresponding author. Fax: +41 1 632 1162.
E-mail address: pirngruber@chem.ethz.ch (G.D. Pirngruber).

0021-9517/$ – see front matter
doi:10.1016/j.jcat.2005.11.012

$$^* + N_2O \rightarrow {}^*\text{–}O + N_2, \quad (5)$$

$$^*\text{–}O + {}^*\text{–}NO_2 \rightarrow {}^* + {}^*\text{–}NO + O_2, \quad (6)$$

Sum: $2N_2O \rightarrow 2N_2 + O_2$.

The beneficial role of NO_2 in O_2 formation is reminiscent of mechanistic studies of NO decomposition over copper zeolites [9,10]. In this system NO_2 enhances the rate of O_2 formation by facilitating the recombination of two remote surface oxygen atoms via transport in the gas phase, that is,

$$^*\text{–}O + NO \rightarrow {}^* + NO_2, \quad (4a)$$

$$NO_2 + {}^*\text{–}O \rightarrow {}^* + NO + O_2. \quad (6a)$$

This sequence is identical to (4) and (6), but involving NO_2 in the gas phase instead of adsorbed NO_2.

In contrast, conventional N_2O decomposition occurs via the recombination of two deposited oxygen atoms on the surface, that is,

$$2^* + 2N_2O \rightarrow 2^*\text{–}O + 2N_2, \quad (7)$$

$$2^*\text{–}O \rightarrow O_2. \quad (8)$$

The enhancement of the N_2O decomposition activity by NO depends on the relative rate of the two catalytic cycles. Recently, Pieterse et al. [11] studied N_2O decomposition in the presence of NO, oxygen, and water over Fe-ZSM-5 samples prepared by wet ion exchange (WIE), chemical vapor deposition (CVD), and steam-activated isomorphous substitution. These authors concluded that WIE resulted in catalysts with the highest N_2O conversion, although containing much less iron than the CVD samples studied. They proposed that the differences observed among the Fe-ZSM-5 samples prepared by the various methods were related to the ability of the predominant iron species to catalyze NO-assisted N_2O decomposition.

To explore this possibility in more detail, we studied the NO-assisted N_2O decomposition over Fe-ZSM-5 samples, prepared by CVD or WIE, from two different parent zeolites. The beneficial effect of NO differed among the samples. By combining characterization data, in situ infrared (IR) spectroscopy and transient response measurements, we offer an explanation for that phenomenon. Furthermore, we discuss the mechanism of NO-assisted N_2O decomposition in detail.

2. Experimental

2.1. Sample preparation

Two parent ZSM-5 samples were used, MFI-P46 (Südchemie; Na-H-ZSM-5, Si/Al = 24, synthesized with template) and SM27 (Alsi Penta/Südchemie; NH_4-ZSM-5, Si/Al = 12, template-free synthesis). MFI-P46 was transformed in the NH_4 form by three-fold exchange with a 1 M NH_4NO_3 solution. The NH_4 form of the samples was used for the CVD of $FeCl_3$ [12] or for WIE with an aqueous solution of $FeSO_4$. For CVD, the samples were first treated in O_2 at 773 K for 1 h; then $FeCl_3$ was sublimed onto the zeolite at 593 K, followed by extensive washing and another calcination at 773 K [13]. WIE was carried out with $FeSO_4 \cdot 7H_2O$ at 353 K for 6 h in N_2 atmosphere, to avoid oxidation of Fe^{2+} to Fe^{3+}. Exchange with Fe^{2+} ions is preferred over exchange with Fe^{3+} ions, because Fe^{3+} ions tend to precipitate as Fe_2O_3 clusters on the outer surface of the zeolite. The exchange solution included 1 mmol of iron per 1 g of NH_4-ZSM-5, Si/Al 12 and 0.5 mmol of iron per 1 g of NH_4-ZSM-5, Si/Al 24. For filtration, 2 × 1000 mL of demiwater per 10 g of cake was poured on the cake while keeping the cake under vacuum. The samples were subsequently dried in an oven at 353 K, then calcined at 773 K for 5 h (at a heating rate of 1 K/min) in static air under shallow bed conditions. During calcination, oxidation of the exchanged Fe^{2+} ions to Fe^{3+} occurs. Ultraviolet–visible light (UV–vis) spectra of the calcined iron zeolites were recorded in diffuse reflection on a Cary 400 UV–vis spectrometer equipped with a Praying Mantis sample stage from Harrick. The Fe and Al content of the samples was determined by atomic absorption spectroscopy after the zeolites were dissolved in HF and HNO_3 (see Table 1).

Table 1
Elemental composition of the samples and fraction of the Brønsted OH groups exchanged against Fe, as determined by IR spectroscopy

Sample	Fe (wt%)	Fe/Al	OH exchange
Fe-ZSM-5-24 WIE	1.0	0.26	0.25
Fe-ZSM-5-24 CVD	4.4	1.1	0.38
Fe-ZSM-5-12 WIE	2.8	0.45	0.47
Fe-ZSM-5-12 CVD	5.4	0.87	0.34

The samples are coded as Fe-ZSM-5-*x*-CVD (WIE), where *x* represents the Si/Al ratio of the parent and CVD or WIE specifies the preparation method.

2.2. Activity measurements

Catalytic tests were carried out in a computer-controlled multiport flow setup. Quartz reactors with an internal diameter of 5 mm were placed in a heated reactor vessel. The catalyst sieve fraction (0.25–0.5 mm) was placed on a quartz grid. Space velocities (GHSV) are reported at room temperature and atmospheric pressure. The feed consisted of 3000 ppm N_2O and 0 or 800 ppm NO, the balance being N_2. Gas purity was 99% for N_2O and 99.8% for NO. The quantitative analysis of N_2O, N_2, and O_2 was performed using a micro gas chromatograph equipped with Poraplot and Molsieve columns and flame ionization and thermal conductivity detectors. NO_x was analyzed with a NO_x (chemoluminescence) analyzer. At the start of each activity experiment, the reactor temperature was increased to 533 K at a rate of 3 K/min under N_2 flow and flushed for 3 h. Then the reaction gas mixture was fed to the catalyst. Preconditioning was set for 20 min at each temperature. Data were collected at ascending temperature using a ramp rate of 5 K/min, to a maximum of 773 K.

2.3. In situ IR spectroscopy

A total of 6 mg of sample was pressed into a self-supporting pellet 6 mm in diameter, placed in a gold sample holder, and

inserted into a cylindrical oven. The oven was screwed onto a stainless steel cell block equipped with gas connections and CaF_2 windows to let the IR beam pass through the cell and the sample. The gas steam flows along the axis of the cylindrical oven through the sample pellet to the exit on the other side. Because the oven does not completely fill the cross-section of the cell, about 10% of the gas bypasses the sample, with the rest flowing through it. The cell represents a reasonable approximation of a plug flow reactor and, because of its small volume, is suited for a rapid switch from one gas mixture to another.

The samples were heated in a stream of 5% O_2 in He at 673 K, then kept for 30 min in a flow of pure He and cooled to reaction temperature (usually 573 K was chosen as the initial temperature). The initial treatment in O_2 serves to remove hydrocarbon impurities, and the subsequent treatment in He allows for partial autoreduction of Fe^{3+} to Fe^{2+}. The reaction was started by switching from He to a mixture of 3000 ppm N_2O and 800 ppm NO in He. NO was purified with a cold trap at 173 K. The reaction was followed for 30 min by IR. The gas phase was simultaneously analyzed by gas chromatography and mass spectrometry; then the feed was switched back to He. The temperature was raised to 673 K for 30 min, and the procedure was repeated at the next temperature. The total gas flow through the cell was kept constant at 20 ml_{NTP}/min. For a 6-mg pellet, this corresponds to GHSV = 120,000 h^{-1} (using a density of 0.5 g/ml).

The IR spectra were recorded on a Biorad FTS 3000 MX spectrometer equipped with a broad band MCT detector. The spectral resolution was 4 cm^{-1}. The catalyst pellet at the reaction temperature in a flow of He was used as background. The ZSM-5-12 samples were not very transparent, which had a negative effect on the signal to noise ratio. The corresponding spectra were Fourier filtered, to reduce the noise. The effluent of the IR cell was monitored by a Omnistar mass spectrometer. m/e values of 4, 28, 30, 32, 44, and 46 were recorded. All signals were normalized to the signal of He ($m/e = 4$), and the concentrations were calculated from a calibration matrix. The low sensitivity of the mass spectrometer for NO_2 did not allow us to obtain reliable NO_2 concentrations. The concentration of NO_2 can be inferred from the difference $c_{N_2} - 2c_{O_2}$. This was verified by a few selected experiments with a NO_x analyzer.

2.4. Transient response measurements

A 50-mg pelletized sample was placed in a 4-mm i.d. quartz tube and treated in a He flow at 673 K for 1 h. The reactor was then cooled to 648 K, and the feed was switched to 800 ppm NO in He. Pulses of 5000 ppm N_2O were given into the flow of NO at intervals of ∼100 s. Then, after letting the system re-equilibrate for 10 min, a step to 3000 ppm N_2O in He was performed. The reaction was followed for ∼30 min, after which the feed was stepped back to NO and finally once again to N_2O. The procedure was repeated at 673 K. The total flow rate in the experiments was 50 ml NTP/min, corresponding to GHSV = 30,000 h^{-1}. The reaction products were analyzed by mass spectrometry as described earlier.

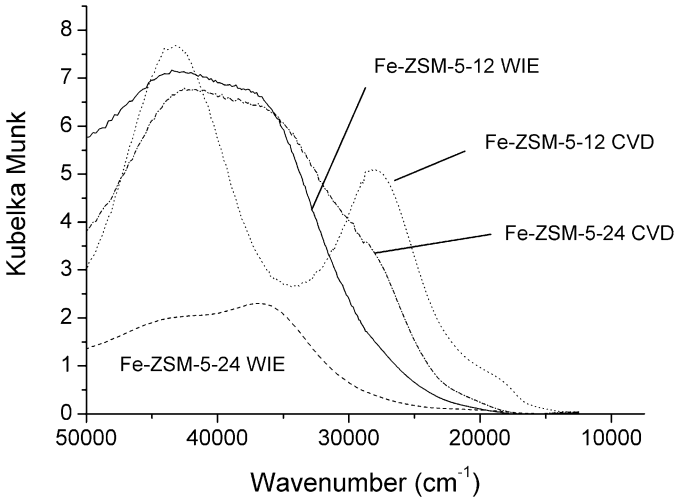

Fig. 1. UV-vis spectra of Fe-ZSM-5-12/24 CVD and WIE.

3. Results

3.1. UV–vis

The UV–vis spectra of both WIE samples (Fig. 1) showed only two intense ligand-to-metal charge transfer bands at 43,000 and 38,000 cm^{-1}, as was expected for isolated iron ions [14]. In the Fe-ZSM-5-24 CVD sample, a shoulder appeared at 27,000 cm^{-1}, indicating clustering of iron atoms [15]. Absorption at 20,000 cm^{-1} demonstrated that some Fe_2O_3 particles were also present. In the UV-vis spectrum of Fe-ZSM-5-12 CVD, the band of Fe_2O_3 was more intense. The spectrum of Fe-ZSM-5-12 CVD differed from the others in that it was dominated by two intense bands at 28,000 and 43,000 cm^{-1}. The position of the bands suggests an assignment to Cl → Fe charge transfer transitions [16]; that is, the chloride could not be completely removed by the repeated washing and calcination of that sample. Note that the band at 28,000 cm^{-1} was observed earlier on a Fe-ZSM-5-12 sample prepared from the same parent zeolite using a $FeCl_2$ precursor, but in our opinion was erroneously assigned to binuclear iron species [17].

3.2. IR spectroscopy

The IR spectra of the parent zeolites ZSM-5-12 and ZSM-5-24 showed distinct differences (Fig. 2). ZSM-5-24 had two intense bands in the region of the OH stretching vibrations, at 3735 cm^{-1} (silanol groups) and at 3600 cm^{-1} (Brønsted OH groups). A very weak band at 3660 cm^{-1} was attributed to Al–OH groups on extra-framework species. In the case of ZSM-5-12, the Brønsted OH band was more intense, due to the higher Al concentration, and the silanol band was very weak. The two bands at 3735 and 3715 cm^{-1} were assigned to external and internal silanol groups [18]. After ion exchange, the intensity of the Brønsted OH band decreased (see Table 1). In the ion-exchanged samples, the fraction of exchanged OH groups corresponds to the Fe/Al ratio; that is, one Fe atom exchanged for one Brønsted site, as has been observed for Cu^{2+} [19,20]. For reasons of charge balancing, the iron must

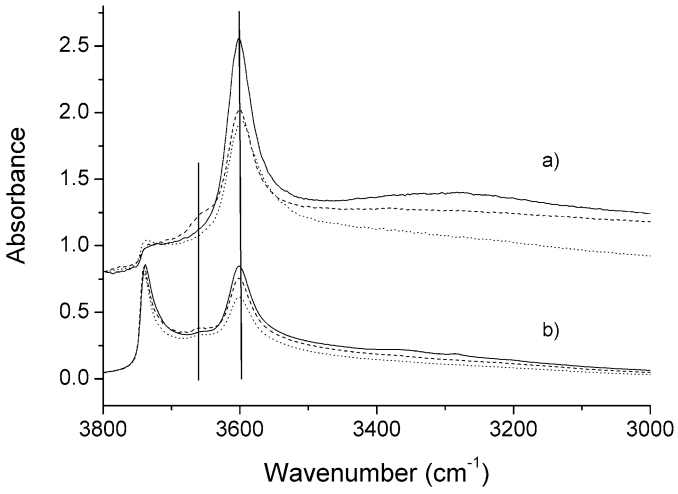

Fig. 2. IR spectra of the dehydrated samples measured at 523 K. (a) ZSM-5-12 parent (solid), WIE (dash), CVD (dotted); (b) ZSM-5-24 parent (solid), WIE (dash), CVD (dotted).

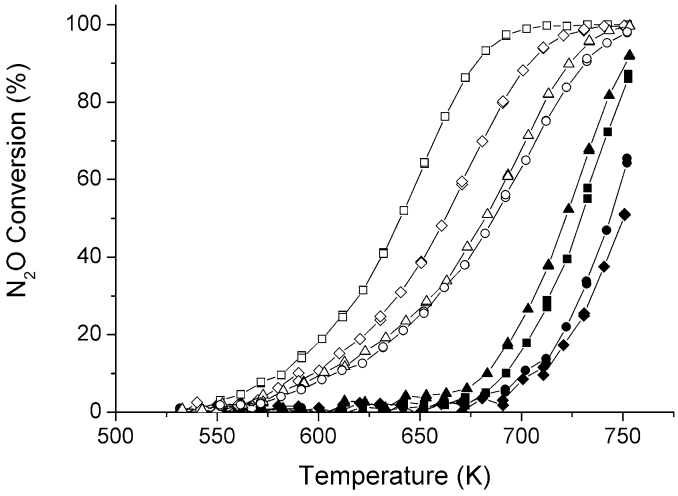

Fig. 3. N_2O decomposition activity of the samples. Feed 3000 ppm N_2O, 0 or 800 ppm NO (full and open symbols), balance N_2, GHSV = 60,000 h^{-1}. ZSM-5-12 WIE (squares), ZSM-5-24 WIE (diamonds), ZSM-5-12 CVD (triangles), ZSM-5-24 CVD (circles).

be bound as $[Fe(OH)_2]^+$. If a dimer bridging two ion-exchange sites is formed, then charge balancing can also be achieved by $[OH–Fe–O–Fe–OH]^{2+}$ or $[OH–Fe\text{-}\mu\text{-}(OH)_2–Fe–OH]^{2+}$. The vibration of the Fe–OH groups can be recognized as a broad band at 3660 cm^{-1} in the spectra of both ion-exchanged samples (Fig. 2). In the CVD samples, on average three iron atoms were bound to one Al site in the form of small iron oxide clusters. Earlier studies reported exchange degrees corresponding to roughly two iron atoms per one Al atom for the CVD method [21,22].

3.3. Comparison of catalytic activity

A comparison of the N_2O decomposition activity of the samples reveals two trends (Fig. 3): Si/Al = 12 > Si/Al = 24 and CVD > WIE. In essence, activity increased with the iron loading of the samples. Adding NO changed the situation. The activity of the WIE samples was strongly boosted by NO, and these samples became significantly more active than the CVD samples, despite their lower iron loading. For a semiquantitative description, we compared the temperatures at which the catalysts reached a N_2O conversion of 20% (Table 2). Adding NO shifted the activity curve by −100 K for the WIE samples and by −80 and −60 K for the CVD samples with Si/Al = 24 and 12, respectively.

Table 2
Temperature at which the catalysts reach a N_2O conversion of 20%. Feed concentration 3000 ppm N_2O, 0 or 800 ppm NO, GHSV = 60,000 h^{-1}

	with NO	without NO	ΔT
Fe-ZSM-5-12 WIE	331	432	−101
Fe-ZSM-5-24 WIE	350	451	−101
Fe-ZSM-5-12 CVD	360	422	−62
Fe-ZSM-5-24 CVD	367	447	−80

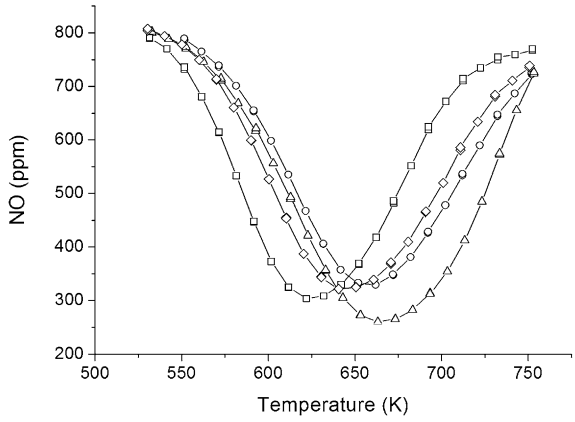

Fig. 4. NO concentration profile. Feed 3000 ppm N_2O, 800 ppm NO, balance N_2, GHSV = 60,000 h^{-1}. ZSM-5-12 WIE (squares), ZSM-5-24 WIE (diamonds), ZSM-5-12 CVD (triangles), ZSM-5-24 CVD (circles).

The NO concentration profile shows how NO influences the conversion of N_2O (Fig. 4). When the temperature is raised, the concentration of NO decreases and NO_2 is produced (not shown). NO_2 is formed not through reaction of NO with O_2, originating from decomposition of N_2O, but rather by direct reaction with N_2O [8], that is,

$$NO + N_2O \rightarrow NO_2 + N_2. \quad (9)$$

Most of the N_2O conversion in temperature range 550–650 K is due to this stoichiometric reaction of NO with N_2O (see Fig. 5). Above ∼650 K, the effect of NO becomes mainly catalytic. N_2O decomposition strongly increases, and NO concentration increases once again.

3.4. In situ IR spectroscopy

In situ IR spectroscopy was used to explain the different activity of the four samples based on the nature and concentration of adsorbed surface species. Thin catalyst pellets were exposed to a flow of 3000 ppm N_2O and 800 ppm NO in He. The space velocity in these experiments was a factor of two lower than in the activity measurements described above. The adsorbed

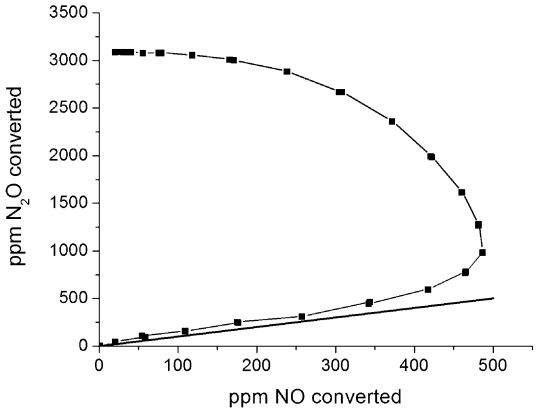

Fig. 5. Conversion of N_2O vs. conversion of NO. Solid line corresponds to a conversion of one N_2O per NO. Fe-ZSM-5-12 WIE, GHSV = 60,000 cm^{-1}.

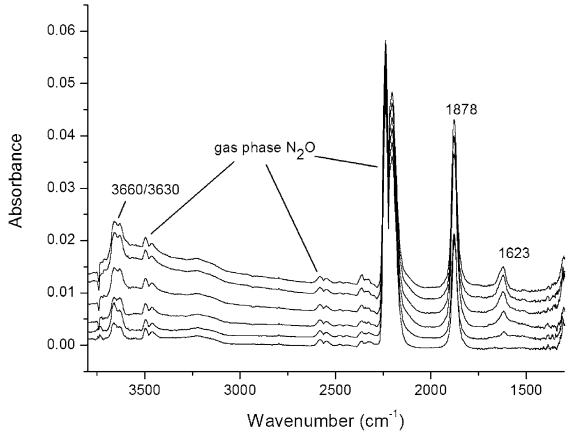

Fig. 6. Time evolution of IR spectra of adsorbed species on Fe-ZSM-5-24 WIE at 573 K during reaction with 3000 ppm N_2O and 800 ppm NO. Fe-ZSM-5-24 spectra after 30 s, 1, 2, 4 and 19 min (each offset by 0.002). GHSV = 120,000 h^{-1}.

species were characterized in the temperature range of 573–648 K, the range in which first the stoichiometric reaction and then the catalytic reaction between NO and N_2O set in.

Fig. 6 shows the time evolution of the spectra measured for Fe-ZSM-5-24 WIE at 573 K. A nitrosyl band at 1878 cm^{-1} increased rapidly, in parallel with the concentration of NO in the gas phase. After 4 min, the nitrosyl band reached its maximum intensity and then decreased slightly. A band at 1623 cm^{-1} increased gradually with time. According to its wavenumber, this band can be assigned to a nitrato (NO_3^-) or a weakly bound nitro group (NO_2) [23,24]. The band disappeared rapidly when switching from the reaction mixture to He. Thus we assigned the band to a weakly bound NO_2 species [25] rather than to a NO_3^- group, which would have greater thermal stability. The appearance of the nitro band indicates that oxidation of NO to NO_2 occurred. As expected from the stoichiometry of reaction (9), a higher concentration of N_2 was observed in the gas phase during the buildup of NO_2 on the surface.

The doublets at 3498/3464, 2583/2547, and 2238/2208 cm^{-1} were due to gas-phase N_2O. A low-frequency tail of the 2208 cm^{-1} band can be attributed to NO^+ species, but its concentration was much lower than in a feed of NO + O_2 [26].

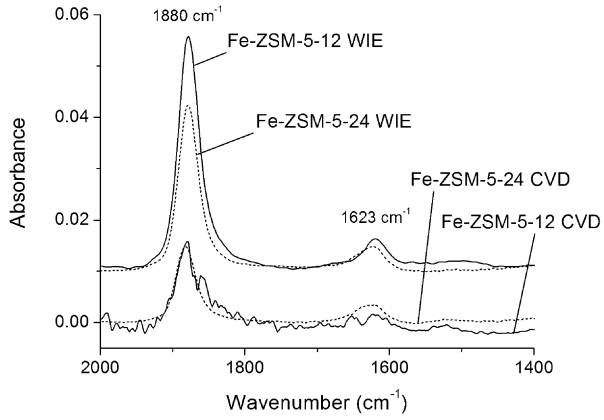

Fig. 7. IR spectra after 30 min in 3000 ppm N_2O + 800 ppm NO at 573 K.

In addition, new bands emerged in the high-frequency region of the spectrum. The most intense band was a doublet at 3660 and 3630 cm^{-1} (Fig. 6). These bands were observed before and during reaction of N_2O with Fe-ZSM-5 and were assigned to a $Fe(OH)_2$ group [27]. They were generated during the oxidation of Fe^{2+} to Fe^{3+} [28]. The source of the additional OH-groups must be traces of water in the feed. The OH bands did not appear when only NO was flown over the catalyst.

Fig. 7 compares the spectra of the four investigated catalysts in the region of the relevant NO_x vibrations. The two WIE samples exhibited more intense nitrosyl bands than the two CVD samples. The intensity of the nitro band was similar on all catalysts. On Fe-ZSM-5-12 WIE, an additional broad absorption was found at ∼1500 cm^{-1}. The wavenumber suggests assignment to a surface nitrito species, that is, a –O–N=O$^-$ group bound to surface area via the oxygen atom [23]. The band did not disappear when switching to He, supporting the assignment to a strongly bound charged species. The CVD samples exhibited a weak band at 1530 cm^{-1}. This band had high thermal stability and thus must be due to a charged species (nitrito or nitrato), although it was not exactly assigned. $Fe(OH)_2$ bands at 3660 and 3630 cm^{-1} were found on both catalysts prepared by WIE (not shown). On the CVD samples, only a broad band due to hydrogen-bonded hydroxyls appeared, due to the higher density of iron sites on the CVD materials.

A control experiment with the parent ZSM-5-12 sample (600 ppm Fe) yielded entirely different spectra. No new OH stretching vibrations were observed. A weak nitrosyl band was formed due to adsorption of NO on the Fe impurities or on Al^{3+} [29], but the intensity of the nitrosyl band was 10 times weaker than on Fe-ZSM-5-12 WIE. Further, a multitude of bands was formed between 1800 and 1300 cm^{-1}, attributed to surface nitro, nitrato, and nitrito groups. These bands were highly stable on the catalyst surface and behaved like spectators when switching from the reaction mixture to He and back. The behavior of the parent was completely different in the CVD and WIE samples. Activity tests in the plug flow reactor showed that the activity of the parent sample was negligible compared with that of Fe-ZSM-5. Therefore, we can state that (a) the catalysis runs on the iron cations (clusters), which were introduced by exchange, and that (b) the in situ IR measurements probe the

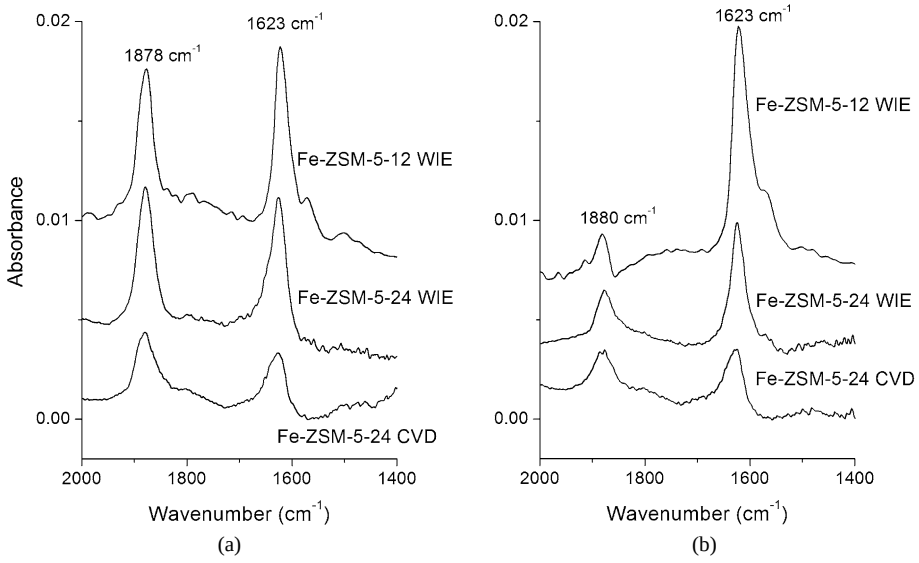

Fig. 8. IR spectra after 30 min in 3000 ppm N_2O + 800 ppm NO at (a) 623 K and (b) 648 K.

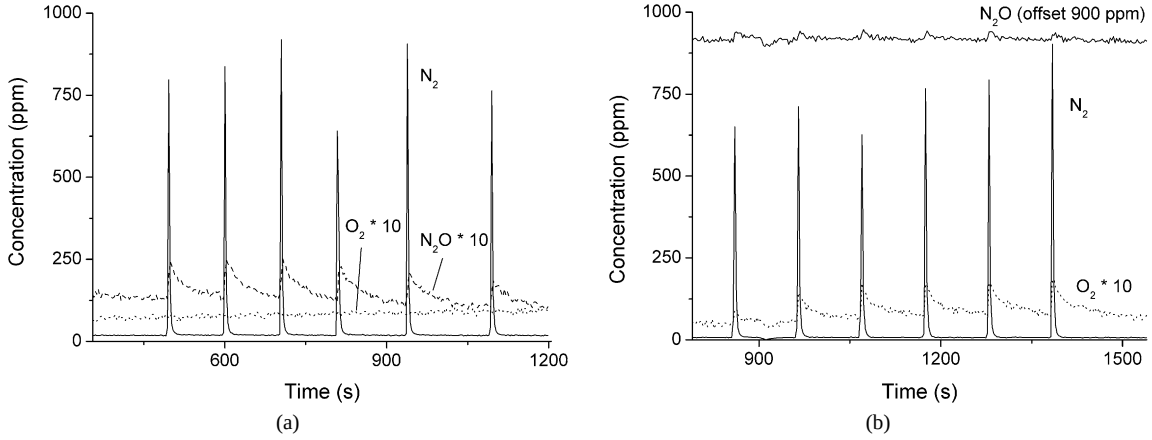

Fig. 9. Pulses of 5000 ppm N_2O into a flow of 800 ppm NO at (a) 648 K and (b) 673 K. Fe-ZSM-5-12 WIE, GHSV = 30,000 h^{-1}.

adsorption/reaction on these iron sites, not on the zeolite matrix.

The adsorbed species on Fe-ZSM-5 reached steady state much quicker at 623 K than at 573 K (not shown). The intensity of the nitrosyl bands at 1880 cm^{-1} stabilized at a value approximately a factor of five lower than at 573 K (see Fig. 8a). In contrast, the intensity of the NO_2 band increased for the two WIE samples and remained roughly constant for Fe-ZSM-5-24 CVD. Due to the high noise level of the spectrum, Fe-ZSM-5-12 CVD was not included in the comparison. In addition to the nitrosyl and nitro bands, Fe-ZSM-5-12 WIE exhibited absorption at 1570 and at 1500 cm^{-1}. In analogy to Cu-ZSM-5, the former band can be assigned to chelating nitrate species (see Scheme 1) [30,31], and the latter is due to nitrite species (*vide supra*).

When switching from the reaction mixture back to He, the nitrosyl band disappeared very quickly (in parallel with the decreased NO concentration in the gas phase). In the case of Fe-ZSM-5-12 WIE, the nitro band also disappeared within a few minutes. For the other catalysts, a fast initial decrease of the nitro band was observed, but a band at 1630 cm^{-1} remained and decreased only very slowly with time. This finding demonstrates that the nitro groups on Fe-ZSM-5-12 WIE are very labile, whereas part of the surface nitro groups on the other catalysts have rather high thermal stability.

At 648 K, the nitrosyl band further decreased in intensity compared with at 623 K (see Fig. 8b). The intensity of the nitro band increased for Fe-ZSM-5-12 WIE and slightly decreased for the other samples. The intensity of the NO_2 band at 648 K follows the order Fe-ZSM-5-12 WIE > Fe-ZSM-5-24 WIE > Fe-ZSM-5-24 CVD > Fe-ZSM-5-12 CVD. The same order can be obtained at 623 K if only the labile nitro groups (i.e., those that desorb within 1 min in He) are counted. Note that the intensity of the nitrosyl band at lower temperatures (573 K) follows the same order.

The N_2O conversions measured in the in situ IR experiments were approximately a factor of 10 lower than those measured in the plug flow reactor. At 573 K, hardly any measurable activity was observed in the IR cell; at 648 K, conversions ranged from 2 to 7%.

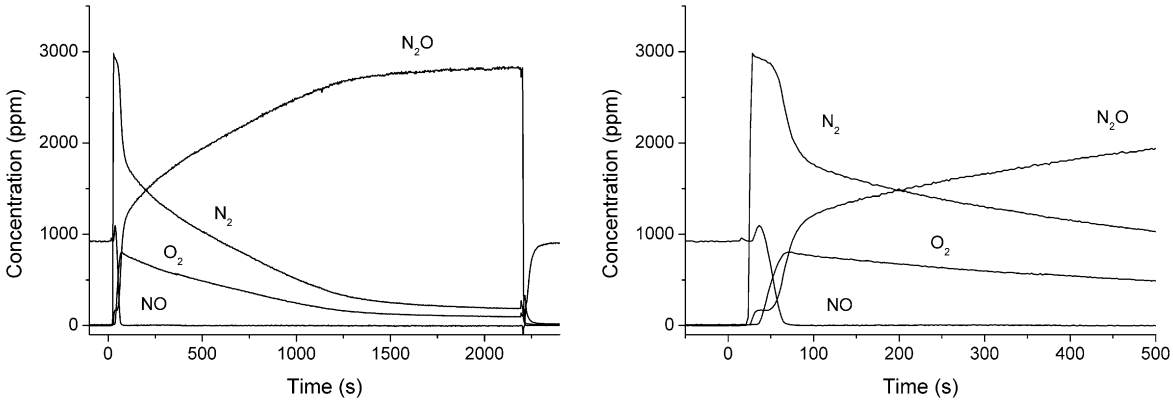

Fig. 10. (a) Step from 800 ppm NO to 3000 ppm N_2O in He at 648 K and step back to NO. (b) Zoom of the first 500 s after the step. Fe-ZSM-5-12 WIE, GHSV = 30,000 h^{-1}.

3.5. Pulse and step experiments

To obtain more insight into the reactivity of the surface species, pulse and step experiments were performed in a tubular quartz reactor at 648 and 673 K and in the IR reactor at 648 K. The space velocity in the IR reactor was roughly a factor of four lower than that in the plug flow reactor.

When N_2O was pulsed into a flow of NO over the catalyst Fe-ZSM-5-12 WIE, a peak of N_2 was formed (see Fig. 9). A peak of O_2 was detected at 673 K, but not at 648 K. The O_2 peak strongly tailed with respect to the N_2 peak. The same phenomenon was observed in earlier TAP experiments [8]. In the IR reactor, the nitrosyl band at 1880 cm^{-1} decreased during the N_2O pulse and regained its original intensity after the pulse; that is, some NO was replaced by the incoming N_2O. No nitro bands were detected. It is interesting to note that the pulse of N_2O was strongly broadened and tailed, especially at 648 K. This indicates that some N_2O was molecularly adsorbed on the iron sites. The effect was observed on both WIE catalysts, but not on Fe-ZSM-5-24 CVD. Fe-ZSM-5-24 CVD also did not produce any O_2 during the N_2O pulses, even at 673 K.

After the pulses of N_2O, a step from NO to N_2O was performed (see Fig. 10). A peak of N_2 was produced immediately after the step. This peak of N_2 was not related to NO_2 formation, but rather was due to the reoxidation of Fe^{2+} sites to Fe^{3+} [32]. NO was desorbed from the catalyst (indicated by the peak of NO in Fig. 10b), being replaced by N_2O. After some delay, the production of O_2 began. After 40 s, N_2 and O_2 decayed in parallel to the steady-state value. The steady-state activity was due to NO-unassisted N_2O decomposition.

The delayed onset of O_2 formation, followed by the simultaneous decay of N_2 and O_2, were also observed in the IR reactor (Fig. 11). Due to the higher space velocity, less O_2 was formed. The intensity of the surface nitrosyl band decreased in parallel with the gas-phase concentration of NO. A desorption peak of NO, as in the tubular quartz reactor, was not observed, again due to the high space velocity. With a delay of ∼10 s (similar to the delay of O_2 formation), a nitro band was formed. The nitro band increased in intensity as long as NO was still present in the gas phase and then slowly decreased. Fig. 11 shows that

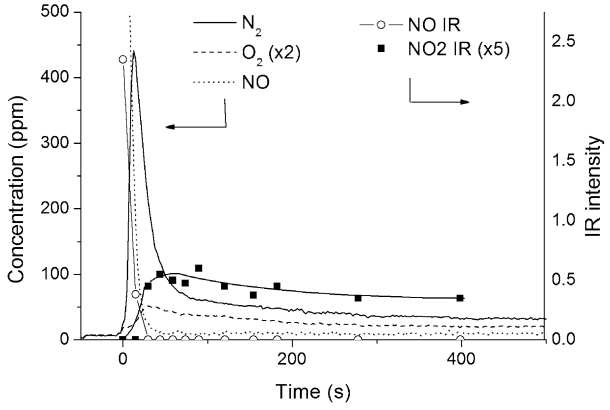

Fig. 11. Step from 800 ppm NO to 3000 ppm N_2O in He at 648 K in the IR reactor. Intensity of the nitrosyl band (circles) and of the NO_2 band (×5, squares) on right axis. Gas phase concentration of N_2 (solid), NO (dotted), and O_2 (×2, dashed). Fe-ZSM-5-12 WIE, GHSV ∼120,000 h^{-1}.

Table 3
Quantification of the initial peak of N_2 formed after a step from 800 ppm NO to 3000 ppm N_2O in He, at 648 or 673 K, as well as of the amount of O_2 formed in the subsequent N_2O decomposition. GHSV = 30,000 h^{-1}

	N_2 peak (μmol)	O_2[a] (μmol)	N_2 peak (mol/mol Fe)	O_2[a] (mol/mol Fe)
648 K				
Fe-ZSM-5-12-WIE	3.7	15	0.15	0.59
IR reactor[b]			0.14	0.07
Fe-ZSM-5-24-WIE	1.9	2.0	0.22	0.23
Fe-ZSM-5-24-CVD	0.7	0	0.02	0
673 K				
Fe-ZSM-5-12-WIE	1.21	21	0.05	0.85
Fe-ZSM-5-24-WIE	0.9	4.7	0.11	0.54
Fe-ZSM-5-24-CVD	0.5	0	0.01	0

[a] Steady state activity, due to NO-unassisted N_2O decomposition, subtracted.
[b] GHSV ∼ 120,000 h^{-1}.

the evolution of the NO_2 band and the formation of O_2 in the gas phase were synchronized.

The behavior of the other catalysts was studied only in the tubular quartz reactor. Fe-ZSM-5-24 WIE behaved qualitatively like Fe-ZSM-5-12 WIE, but its activity for O_2 formation after the step was lower (Table 3). With Fe-ZSM-5-24 CVD, no

accelerated O_2 formation was observed. The activity settled immediately at its steady-state value, due to unassisted N_2O decomposition.

After the step back from N_2O to NO, a small peak of O_2 and an even smaller peak of N_2 were observed. The O_2 formation decayed in less than 80 s. The amount of O_2 formed decreased from 0.015 mol/mol Fe in Fe-ZSM-5-12 WIE to 0.008 mol/mol Fe in Fe-ZSM-5-24 WIE to 0.001 mol/mol Fe in Fe-ZSM-5-24 CVD. In the IR reactor, a nitro band increased and decayed simultaneously with the O_2 peak.

4. Discussion

4.1. Structure of the iron sites in WIE and CVD catalysts

The UV–vis and IR spectra suggest that the WIE samples contain isolated iron cations located at ion exchange positions. However, recent EXAFS data indicate that iron dimers can be formed at high ion exchange degrees [33], as has been reported for Cu-ZSM-5 [34]. Because the Fe/Al ratio of our WIE samples is rather high (Fe/Al = 0.26 and 0.45), we suspect that a mixture of isolated sites and dimers is present. Several studies have shown that the CVD samples contain small oligomeric iron oxide clusters [35–37]. This is confirmed by the UV–vis and IR data presented here.

4.2. The adsorbed species

The dominating surface species in our experiments are mononitrosyl species (1880 $cm^{-1)}$ and adsorbed NO_2 (1625 cm^{-1}). Both bands were also observed in a similar study by Mul et al. [7], although that study was performed at lower temperatures. The stretching frequency of the nitrosyl band is only slightly higher than the stretching frequency of NO in the gas phase (1876 cm^{-1}), indicating a very weak coordinative bond of NO to iron. When NO adsorption is studied at room temperature, a multitude of bands, assigned to dinotrosyl and trinitrosyl species [38] or to mononitrosyls adsorbed in different positions in the ZSM-5 host [39], is observed. At the high temperatures used in our in situ experiments, NO does not discriminate between these sites, and only a single band is observed. It is generally agreed that NO adsorbs rather strongly on Fe^{2+} but only weakly or not at all on Fe^{3+} [23,38]. Test experiments confirmed that catalysts that were not allowed to autoreduce in He before switching to the reaction mixture adsorbed less NO. We therefore assign the band at ∼1880 cm^{-1} to mononitrosyl species bound to Fe^{2+} [40].

The second prominent band in the spectra is the nitro band at 1625 cm^{-1}. In the Fe-ZSM-5-12 WIE sample, the band exhibits a shoulder at 1575 cm^{-1} at higher temperatures. A similar pair of bands at 1625 and 1575 cm^{-1} is observed when NO + O_2 is passed over a Fe-ZSM-5 catalyst [25,41]. When formed from NO + O_2, the band at 1625 cm^{-1} has rather high thermal stability, and is probably due to a bridging nitrate species rather than to an adsorbed nitro group. The two groups vibrate at very similar wavelengths and can be distinguished based solely on their thermal stability. At high concentrations (>1%), bands at 1625 and 1575 cm^{-1} can also be formed from N_2O [42,43]. In the concentration and temperature range used in our study, however, N_2O does not create any strongly IR absorbing surface species [44]. Therefore, the source of the nitro/nitrate bands at 1625 and 1575 cm^{-1} in our experiments must be the oxidation of NO by N_2O. These bands are also formed on reaction of NO + O_2 on our catalysts, but the intensity and thermal stability differ.

4.3. The role of the surface species in the reaction mechanism

Two different models have been proposed to explain the catalytic effect of NO on N_2O decomposition, one involving nitrito and nitrato species [6] and the other involving adsorbed NO_2, which functions as an intermediate oxygen storage [7,8]. In our in situ IR experiments, bands of adsorbed NO_2 (∼1625 cm^{-1}), chelating nitrates (1575 cm^{-1}), and weak bands of nitrito species were observed. The band of molecularly adsorbed NO_2 was by far the most intense, and its intensity at high temperatures correlated with the catalytic activity of the samples (Fig. 12). During the step experiments (i.e., during a step from NO to N_2O), the NO_2 band appeared as the only new surface species, and its intensity correlated with the O_2 formation. These three results prove that adsorbed NO_2 is indeed part of the catalytic cycle of NO-assisted N_2O decomposition, as proposed by Perez-Ramirez et al. [8]. We return later to the question of whether the chelating nitrate (1575 cm^{-1}) also plays a role in the reaction mechanism.

With the help of our transient response experiments, we can extract more details of the catalytic cycle described in Eqs. (3)–(6). When N_2O was pulsed into a flow of NO, unreacted N_2O was rather strongly retained on the WIE catalysts; that is, it was molecularly adsorbed (Fig. 9). After a step of NO to N_2O, N_2O partially replaced NO from the adsorption sites, leading to the peak of NO observed in Fig. 10b. These two findings suggest that N_2O adsorbs molecularly on the WIE catalysts and that N_2O competes with NO for adsorption sites. After the step from N_2O to NO, NO_2 species were formed only as long as N_2O was still present in the gas phase. We therefore propose that, instead of adsorbed oxygen atoms, molecularly adsorbed N_2O is involved in the formation of NO_2 on the WIE catalysts. We can write the reaction mechanism as

$$Fe^{2+}(NO) + N_2O \rightarrow Fe^{2+}(NO)(N_2O) \rightarrow Fe^{2+}(NO_2) + N_2, \quad (11)$$

$$Fe^{2+}(NO_2) + N_2O \rightarrow Fe^{2+}(NO) + N_2 + O_2. \quad (12)$$

After the step from NO to N_2O, N_2O replaces NO from adsorption sites, as was also observed by Mul et al. [7]. Then NO_2 is formed by reaction of adsorbed NO with N_2O [reaction (11)], which is adsorbed on the same site or on a neighboring iron site (if the iron sites are dimers). The concentration of adsorbed NO_2 reaches its maximum when the gas-phase NO concentration decreases to zero. After that, the build-up of NO_2 by reaction (11) ceases, and only its consumption by reaction (12) follows. Reaction (12) should restore adsorbed NO on the surface. However, adsorbed NO was not observed 50 s after the step to N_2O (Fig. 11). The reason is that adsorbed NO, once

regenerated by reaction (12), is rapidly reoxidized to NO_2 by reaction (11). In contrast, the consumption of NO_2 by reaction (12) is slow. This is in line with earlier work, which concluded that O_2 formation is the rate-limiting step of the reaction [7,8]. Instead of being oxidized to NO_2 and refed to the catalytic cycle, the adsorbed NO can also desorb into the gas phase. This process terminates the catalytic cycle and leads to the slow decay of the catalytic activity when NO is not present in the feed. The competition between oxidation of NO to NO_2, and its desorption from the surface determines how much O_2 can be formed after the step from NO to N_2O.

In contrast to the WIE samples, enhanced N_2 formation after the step from NO to N_2O was not observed for the CVD catalyst (see Table 3). The replacement of adsorbed NO by N_2O, resulting in a desorption peak of NO, also was not observed. We presume that on the CVD catalyst, N_2O adsorbs and dissociates on sites remote from the NO adsorption sites. The deposited oxygen atom has to migrate to the adsorbed NO to form NO_2. This process is slower than the direct reaction of adsorbed NO with N_2O on the WIE catalysts; hence significant amounts of NO_2 are not formed in the step experiment with the CVD catalyst and enhanced N_2 formation is not observed. Note, however, that NO_2 formation is not the rate-limiting step in steady state. Therefore, the slower NO_2 formation on the CVD catalysts cannot explain their lower activity in NO-assisted N_2O decomposition.

It is worthwhile to analyze O_2 formation [reaction (12)], which is rate-determining, in more detail. Different mechanistic pathways can be considered.

Option 1:

$$\mathrm{Fe^{2+}(NO_2) + N_2O \rightarrow Fe^{2+}(NO_2)(N_2O)} \rightarrow \mathrm{Fe^{2+}(NO) + N_2 + O_2}. \quad (12a)$$

Option 2:

$$\mathrm{N_2O + Fe^{2+} \rightarrow Fe{-}O + N_2}, \quad (12b)$$
$$\mathrm{Fe{-}O + Fe^{2+}(NO_2) \rightarrow Fe^{2+}(NO) + O_2}.$$

Option 3:

$$\mathrm{N_2O + Fe^{2+} \rightarrow Fe{-}O + N_2}, \quad (12c)$$
$$\mathrm{Fe^{2+}(NO_2) \rightarrow Fe^{2+} + NO_2},$$
$$\mathrm{Fe{-}O + NO_2 \rightarrow Fe{-}O(NO_2) \rightarrow Fe^{2+}(NO) + O_2}.$$

The first option is a direct reaction of N_2O with adsorbed NO_2, possibly through an intermediate in which both molecules are adsorbed on the same iron site [45]. Alternatively, N_2O may first dissociate into N_2 and an adsorbed oxygen atom. If the oxygen atom is deposited in the vicinity of adsorbed NO_2 or if it has the potential to migrate, it can react with NO_2 to give O_2 and adsorbed NO [reaction (12b)]. This is in essence the mechanism proposed by Perez-Ramirez et al. [8]. A third possibility is that NO_2 desorbs into the gas phase and reacts with an oxygen atom deposited from N_2O. The band at 1575 cm^{-1} can be tentatively ascribed to the intermediate formed between the deposited surface oxygen atom and a gas-phase NO_2 molecule

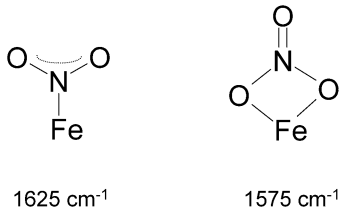

Scheme 1. Structures of adsorbed NO_2 and of chelating nitrate.

(see Scheme 1), which then decomposes to NO and O_2. A similar role of transporting oxygen atoms between distant sites to facilitate O_2 formation has been attributed to NO_2 in the decomposition of NO over Cu-ZSM-5 [9,10]. Note that the first and last pathways can operate on isolated iron sites, whereas the second pathway requires the presence of two iron sites for the adsorption of oxygen and of NO/NO_2, which are located near each other, that is, a dimer or an even larger iron cluster.

Can we determine whether the contribution of adsorbed NO_2 or that of gas-phase NO_2 dominates on the iron zeolites? Perez-Ramirez et al. [8] showed that when NO and N_2O were alternately pulsed over the catalyst at 773 K, NO_2 appeared in the gas phase only during the NO pulses, but O_2 was formed after the pulses of N_2O, that is, when NO_2 was not present in the gas phase. This finding speaks in favor of adsorbed NO_2. Our results show that the activity of the catalysts is correlated with the concentration of adsorbed NO_2 at 648 K. Keep in mind, however, that at 648 K the effect of NO/NO_2 on N_2O decomposition is still mainly stoichiometric and not catalytic. The catalytic effect of NO becomes more dominating at higher temperatures. Under these conditions, we can expect the adsorption of NO_2 on the surface to be weak and the gas-phase mechanism to certainly gain in importance.

4.4. Comparison of CVD and WIE samples

The IR measurements at 573 K correspond to a situation in which conversion is close to zero. The concentration of adsorbed NO under these conditions correlates with the activity of the samples at higher temperatures (Fig. 12). NO adsorbs preferentially on Fe^{2+}. The concentration of Fe^{2+} on the samples can be estimated from the initial peak of N_2, which was always observed in the step experiments. The peak of N_2 is related to reoxidation of Fe^{2+} to Fe^{3+}, according to the equation

$$\mathrm{2Fe^{2+} + N_2O \rightarrow 2Fe^{3+} + O^{2-} + N_2}. \quad (13)$$

We chose the values obtained in the steps from NO to N_2O (see Table 3) (which are more precise than those of in the in situ IR experiments) and used the Fe^{2+}/N_2 stoichiometry of reaction (13). The concentration of Fe^{2+} determined by this method correlates with the concentration of adsorbed NO (Fig. 13). At higher temperatures (i.e., with increasing N_2O conversion), an increasing fraction of adsorbed NO is converted into adsorbed NO_2. The more NO is adsorbed on the catalyst under nonreactive conditions, the more can be converted to NO_2 at higher temperatures (Fig. 12) and thereby contribute to the increased catalytic activity.

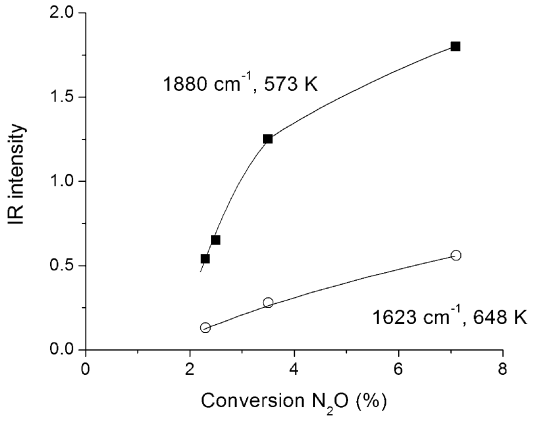

Fig. 12. Intensity of the nitrosyl band at 1880 cm^{-1} at 573 K and of the nitro band at 1623 cm^{-1} at 648 K vs. the N_2O conversion at 648 K (in the IR reactor, i.e., at GHSV ∼120,000 h^{-1}).

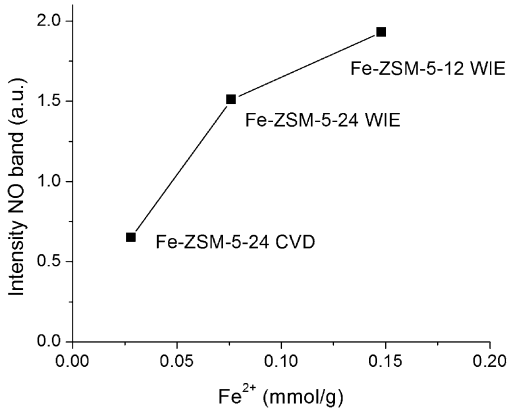

Fig. 13. Normalized intensity of the NO band at 1880 cm^{-1} obtained in the IR experiments at 573 K (normalized by thickness of pellet) vs. concentration of Fe^{2+} sites (values derived from Table 3, 648 K).

The addition of NO to the feed enhances the N_2O decomposition activity of the WIE catalysts more than that of the CVD samples. Fig. 13 shows that the WIE samples have a significantly higher concentration of Fe^{2+} than the CVD samples, despite the higher iron loading of the latter. WIE samples autoreduce more readily than catalysts prepared by CVD [46]. The higher concentration of Fe^{2+} leads to a higher concentration of adsorbed NO/NO_2 on the WIE samples and explains why the WIE samples are more active in NO-assisted N_2O decomposition than CVD materials. A second reason may be the contribution of gas-phase NO_2, which allows oxygen atoms that were deposited on distant iron sites to recombine [see reaction (12c)]. Therefore, gas-phase NO_2 is expected to lead to a stronger enhancement of the reaction rate on isolated iron sites than on clustered iron sites, where O_2 recombination is also possible via migration over the cluster.

Along with comparing WIE and CVD, it is interesting to explore the role of the parent zeolite. Fe-ZSM-12-WIE was far more active than the analogous sample prepared from ZSM-5-24. This can be attributed to the higher iron loading of the former sample (see Table 1). If activity is normalized by the iron loading, then the two samples are similar. Therefore, the high activity of Fe-ZSM-12-WIE is due mainly to the high ion-exchange capacity of the sample, which enables stabilization of a high concentration of isolated iron ions or dimers.

5. Conclusion

NO-assisted N_2O decomposition was studied over Fe-ZSM-5 samples prepared by two different methods (CVD and WIE) from two different parent zeolites. Transient kinetic and IR experiments provided direct proof that adsorbed NO_2 is part of the catalytic cycle of NO-assisted N_2O decomposition. The mechanism of NO_2 formation differs on WIE and CVD samples. On WIE catalysts, NO_2 is formed by the direct reaction of adsorbed NO with N_2O on an isolated iron site or dimer. On CVD samples, containing oligomeric iron species, we presume that NO and N_2O adsorb on distant sites. NO_2 formation is significantly slower. But NO_2 formation is not the rate-limiting step of the reaction. O_2 formation, although strongly accelerated compared with unassisted N_2O decomposition, is still the slowest step of the reaction sequence. O_2 is formed by the reaction of N_2O with adsorbed and/or gas-phase NO_2. The involvement of gas-phase NO_2 is expected to lead to a strong increase in the O_2 formation rate in catalysts containing isolated iron sites, because it facilitates the recombination of oxygen atoms deposited on distant sites. This effect partly explains why WIE samples become more active in NO-assisted N_2O decomposition than the CVD catalysts even though the opposite sequence is found in the decomposition of pure N_2O. But the main reason for the higher activity of the WIE samples is that WIE samples contain a higher concentration of Fe^{2+} sites under reaction conditions. NO preferentially adsorbs on Fe^{2+}, and the concentration of Fe^{2+} determines how many sites take part in the NO-assisted N_2O decomposition cycle.

Acknowledgments

The authors thank Pijus K. Roy (ETH), Saskia Booneveld, and Ruud van den Brink (ECN) for helping to characterize the samples and engaging in helpful discussions.

References

[1] J.T. Houghton, IPCC 3rd assessment report, 2001, http://www.ipcc.ch/pub/reports.htm.
[2] Y. Li, J.N. Armor, Appl. Catal. B 1 (1992) L21.
[3] G. Centi, A. Galli, B. Montanari, S. Perathoner, A. Vaccari, Catal. Today 35 (1997) 113.
[4] G. Centi, S. Perathoner, F. Vazzana, M. Marella, M. Tomaselli, M. Mantegazza, Adv. Environ. Res. 4 (2000) 325.
[5] F. Kapteijn, G. Marban, J. Rodriguez-Mirasol, J.A. Moulijn, J. Catal. 167 (1997) 256.
[6] C. Sang, C.R.F. Lund, Catal. Lett. 73 (2001) 73.
[7] G. Mul, J. Perez-Ramirez, F. Kapteijn, J.A. Moulijn, Catal. Lett. 77 (2001) 7.
[8] J. Perez-Ramirez, F. Kapteijn, G. Mul, J.A. Moulijn, J. Catal. 208 (2002) 211.
[9] B. Moden, P. Da Costa, B. Fonfe, D.K. Lee, E. Iglesia, J. Catal. 209 (2002) 75.
[10] B. Moden, P. Da Costa, D.K. Lee, E. Iglesia, J. Phys. Chem. B 106 (2002) 9633.

[11] J.A.Z. Pieterse, S. Booneveld, R.W. van den Brink, Appl. Catal. B 51 (2004) 215.
[12] H.Y. Chen, W.M.H. Sachtler, Catal. Today 42 (1998) 73.
[13] P.K. Roy, G.D. Pirngruber, J. Catal. 227 (2004) 164.
[14] G. Lehmann, Z. Phys. Chem. Neue Folge 72 (1970) 279.
[15] J. Perez-Ramirez, J.C. Groen, A. Brückner, M.S. Kumar, U. Bentrup, M.N. Debbagh, L.A. Villaescusa, J. Catal. 232 (2005) 318.
[16] P. Marturano, L. Drozdova, G.D. Pirngruber, A. Kogelbauer, R. Prins, Phys. Chem. Chem. Phys. 3 (2001) 5585.
[17] R. Brosius, D. Habermacher, J.A. Martens, L. Vradman, M. Herskowitz, L. Capek, Z. Sobalik, J. Dedecek, B. Wichterlova, V. Tokarova, O. Gonsiorova, Top. Catal. 30/31 (2004) 333.
[18] A. Zecchina, S. Bordiga, G. Spoto, L. Marchese, G. Petrini, G. Leofanti, M. Padovan, J. Phys. Chem. 96 (1992) 4991.
[19] J. Dedecek, B. Wichterlova, J. Phys. Chem. B 101 (1997) 10233.
[20] S.C. Larsen, A. Aylor, A.T. Bell, J.A. Reimer, J. Phys. Chem. 98 (1994) 11533.
[21] P. Marturano, L. Drozdova, A. Kogelbauer, R. Prins, J. Catal. 192 (2000) 236.
[22] A.A. Battiston, J.H. Bitter, F.M.F. de Groot, A.R. Overweg, O. Stephan, J.A. van Bokhoven, P.J. Kooyman, C. van der Spek, G. Vanko, D.C. Koningsberger, J. Catal. 213 (2003) 251.
[23] K.I. Hadjiivanov, Catal. Rev. Sci. Eng. 42 (2000) 71.
[24] K. Nakamoto, Infrared and Raman Spectra of Inorganic and Coordination Compounds, Part B: Applications in Coordination, Organometallic and Bioinorganic Chemistry, 5th ed., John Wiley & Sons, New York, 1997.
[25] L.J. Lobree, I.C. Hwang, J.A. Reimer, A.T. Bell, Catal. Lett. 63 (1999) 233.
[26] K. Hadjiivanov, J. Saussey, J.C. Lavalley, Catal. Lett. 52 (1998) 103.
[27] B.R. Wood, J.A. Reimer, A.T. Bell, M.T. Janicke, K.C. Ott, J. Catal. 225 (2004) 300.
[28] S. Kameoka, T. Nobukawa, S. Tanaka, S. Ito, K. Tomishige, K. Kunimori, Phys. Chem. Chem. Phys. 5 (2003) 3328.
[29] E.J.M. Hensen, Q. Zhu, R.A.J. Janssen, P.C.M.M. Magusin, P.J. Kooyman, R.A. van Santen, J. Catal. 233 (2005) 123.
[30] M.V. Konduru, S.S.C. Chuang, J. Phys. Chem. B 103 (1999) 5802.
[31] M.V. Konduru, S.S.C. Chuang, J. Catal. 196 (2000) 271.
[32] G.D. Pirngruber, J. Catal. 219 (2003) 456.
[33] T. Nobukawa, M. Yoshida, K. Okumura, K. Tomishige, K. Kunimori, J. Catal. 229 (2005) 374.
[34] P. Da Costa, B. Moden, G.D. Meitzner, D.K. Lee, E. Iglesia, Phys. Chem. Chem. Phys. 4 (2002) 4590.
[35] A.A. Battiston, J.H. Bitter, F.M.F. de Groot, A.R. Overweg, O. Stephan, J.A. van Bokhoven, P.J. Kooyman, C. van der Spek, G. Vanko, D.C. Koningsberger, J. Catal. 213 (2003) 251.
[36] E.J.M. Hensen, Q. Zhu, M. Hendrix, A.R. Overweg, P.J. Kooyman, M.V. Sychev, R.A. van Santen, J. Catal. 221 (2004) 560.
[37] G.D. Pirngruber, P.K. Roy, N. Weiher, J. Phys. Chem. B 108 (2004) 13746.
[38] G. Berlier, G. Spoto, G. Ricchiardi, S. Bordiga, C. Lamberti, A. Zecchina, J. Mol. Catal. A 182 (2002) 359.
[39] L.J. Lobree, I.C. Hwang, J.A. Reimer, A.T. Bell, J. Catal. 186 (1999) 242.
[40] G. Mul, J. Perez-Ramirez, F. Kapteijn, J.A. Moulijn, Catal. Lett. 80 (2002) 129.
[41] H.Y. Chen, T. Voskoboinikov, W.M.H. Sachtler, J. Catal. 180 (1998) 171.
[42] E.M. El-Malki, R.A. van Santen, W.M.H. Sachtler, Microporous Mesoporous Mater. 35–36 (2000) 235.
[43] E.M. El-Malki, R.A. van Santen, W.M.H. Sachtler, J. Catal. 196 (2000) 212.
[44] B.R. Wood, J.A. Reimer, A.T. Bell, J. Catal. 209 (2002) 151.
[45] C. Sang, B.H. Kim, C.R.F. Lund, J. Phys. Chem. B 109 (2005) 2295.
[46] G.D. Pirngruber, M. Luechinger, P.K. Roy, A. Cecchetto, P. Smirniotis, J. Catal. 224 (2004) 429.